

DIRECT CURRENT DISCHARGE IN SUPERSONIC FLOW

Valentin A. Bityurin*, Aleksey N. Bocharov* and
Nikolay A. Popov**

*Joint Institute of High Temperatures of Russian Academy of Sciences, Moscow, Russia

**Moscow State University, Moscow, Russia

Key words: Plasma aerodynamics, flow control, drag reduction, DC discharge, supersonic flow

Abstract. In paper¹ the numerical model of non-equilibrium discharge in the flow has been presented based on coupled solution of the Navier-Stokes equations and transport equations for charged particles. This model has been applied to simulate the flow around the spherical cathode reported earlier in experimental work². Conclusion has been drawn that discharge effects on the flow through a thermal mechanism, while electrostatic force appearing in the cathode space charge region is too small to influence the flow field. At the same time, serious discrepancies in the computed and experimental results were observed. It was assumed that these discrepancies are probably due to uncertainties in flow and geometry specifying.

In the current paper an attempt is made to numerically simulate the discharge in the flow for which the free-stream conditions are well known ($Ma = 3.2$). Experimental studies on the discharge under consideration were reported in paper³. The model developed in paper¹ is used for simulations. Attention is paid to the influence of plasma on the supersonic flow. The influence of the discharge on the model's drag is discussed.

Introduction

In paper¹ the numerical model of non-equilibrium discharge in the flow has been presented based on coupled solution of the Navier-Stokes equations and transport equations for charged particles. This model has been applied to simulate the flow around the spherical cathode reported earlier in experimental work². Conclusion has been drawn that discharge effects on the flow through a thermal mechanism, while electrostatic force appearing in the cathode space charge region is too small to influence the flow field. At the same time, serious discrepancies in the computed and experimental results were observed. It was assumed that these discrepancies are probably due to uncertainties in flow and geometry specifying.

In the current paper an attempt is made to numerically simulate the discharge in the flow for which the free-stream conditions are well known. Experimental studies on

the discharge under consideration were reported in paper³. The model developed in paper¹ is used for simulations. Attention is paid to the influence of plasma on the supersonic flow. The influence of the discharge on the model's drag is discussed.

Problem formulation

The longitudinal electric discharge in supersonic flow (Mach number is 3.2) is considered, which has been reported for example in paper³. The interest to this problem is due to the fact that experimental data is complete enough, so one can attempt to compare numerical results with the experimental ones. The computational domain is shown in Fig.1. Cylinder with semi-spherical front-side is positioned in the flow. The cylinder radius is 3 mm, as was in experiments³. It is considered as the cathode. Anode is positioned 14 mm upstream the cathode. In experimental studies anode represented the flat plate as thin as 0.1 mm, which has the sharp tick to initiate the discharge. To avoid severe numerical problems related with resolution of such small scale the anode is assumed to be a circular electrode of diameter of 0.8 mm. One more simplification is that the anode is considered as the boundary for plasma, but not for the main flow. This seems to not significantly influence the computational results. Thus, axi-symmetrical coupled flow/plasma problem described in paper¹ can be considered.

The boundary conditions for flow and plasma equations are specified as follows. At the left and top boundaries of the domain including the anode surface (see Fig.1) the free-stream conditions are set: $(P, U_x, U_y, T) = (1000\text{Pa}; 646 \text{ m/s}; 0; 96\text{K})$, Mach number is 3.2. Here, P is static pressure; U_x is the longitudinal velocity component; U_y – is radial velocity component; T is static temperature. At the right boundary, all flow variables are extrapolated from the interior. On the cylinder surface no-slip and constant temperature conditions are specified, $T = 293\text{K}$. The latter estimate corresponds to adiabatic temperature at the semi-sphere critical point for the flow without the discharge. At the symmetry axis zero normal velocity is specified along with the zero gradients for the other flow variables.

Plasma boundary conditions are as follows. At the cathode surface the boundary conditions are written as $\partial n_i / \partial \mathbf{r}_n = 0$, $(\Gamma_e \mathbf{r}_n) = \gamma_e (\Gamma_i \mathbf{r}_n)$, $\varphi = 0$, where n_i is the ion number density; Γ_e and Γ_i are the electron and ion fluxes specified in [1]; φ is electric potential, and γ_e is secondary emission coefficient, taken as $\gamma_e = 0.05$; \mathbf{r}_n is unit vector normal to the surface. At the anode surface the following conditions are specified: $\partial n_e / \partial \mathbf{r}_n = 0$, $\partial n_i / \partial \mathbf{r}_n = 0$, $\varphi = V$, where n_e is electron number density. Electric potential V is found from the external circuit condition

$$V + R I = E, I = \int_{cathode} \mathbf{j} d\mathbf{S},$$

where E is electromotive force, I is the total current into cathode, and R is the circuit resistance, $R = 30 \text{ kOhm}$. On the rest of boundaries zero gradients are applied for all plasma variables. The discharge is controlled by setting the value of external voltage, E . The flow and plasma fields obtained at some value of external voltage serve as initial conditions for simulations of the discharge at the other, larger value of external voltage.

Results of calculations

Fig.2 represents the distributions of electric potential and total current (sum of electronic and ionic current) obtained for two values of the total cathode current depicted in graphs. It is seen that potential is almost linear over the most part of the discharge gap except for near-electrode regions, especially near-cathode one. Typical voltage drop in the cathode region is about 300V. In addition to “natural” longitudinal non-uniformity of potential related with the occurrence of the positive charge layer near the cathode, there is a “radial” non-uniformity of all the plasma variables near the cathode surface. We assume that this is a typical electrode edge effect: enhanced electric field and current density at the edge of actual electrode. The latter can be specified as the electrode surface through which the current (ionic) comes into electrode. The size of the actual electrode, or cathode spot, is controlled by the effect of so called normal current density. So, the higher total current the larger cathode spot.

Electron and ion number densities fields are shown in Figs.3 and 4. As expected plasma is quasi-neutral overall the discharge gap except for the cathode layer, which is thin enough. One can also see that in general the size of the discharge channel increases with increasing the total current. Distributions of plasma and flow variables along the discharge axis are shown in Fig.5 through Fig.9. In Fig.5 the electron number density is shown for three values of total current. One can see several distinct zones of the discharge. The first zone occupies about 20% of the whole gap and locates near the anode. It is characterized by the highest values of electron number density. These are due to high electric field strength in neutral plasma (very thin negatively charged anode layer does not influence on the discharge significantly). In the case under consideration the so called anode voltage drop is completely due to high resistance of the region near the small-scale electrode. Second, the largest zone spreads up to the shock front. In this zone both concentrations slightly diminish due to the radial expansion of the discharge. Both electron and ion concentrations reveal a small jump on the front of the shock wave due to the drastic change in the gas density. So, a small positive charge locates before shock, and negative charge locates just behind shock. Third zone is between the shock front and the cathode layer. The plasma flow in this zone is determined with three main factors: with essentially non-uniform neutral gas characteristics; with strongly non-uniform distribution of electric field owing to constriction of the discharge to the cathode spot; and dramatic rise of ionization at the outer boundary of cathode layer. Finally, the fourth zone is the positively charged cathode layer. More details on ion distributions near the cathode can be seen from Fig.6. Strictly speaking, plasma is not quasi-neutral within entire shock layer, not only in the cathode one. However, effect of the lack of neutrality in this region on the discharge characteristics is small compared to the effect of cathode layer.

Reduced electric field, E/N , is shown in Fig.7. Typical values of this important quantity in the main discharge are of order of 100 – 150 Td. Small reduction of the reduced field in near-anode zone is due to the rise of density. In turn, the density rises in the anode shock due to high density of heat release. The same reason (increase of density) results in jump-down of the reduced field behind the front of the bow shock. In the cathode layer the reduced electric field can reach the values of order of 3000 Td, which correspond to electric field strength value of 15 kV/cm. Electronic and ionic current densities along the channel axis are presented in Fig.8 and 9, respectively. It is seen that they well correlate with number density distributions shown in Fig.5 and Fig.6.

Some surface distributions of plasma characteristics are shown in Fig.10 and 11. In these plots angle coordinate is used as abscissa. As the total current increases the cathode spot increases too, and all distributions become more and more uniform within the spot. That is, two-dimensional effect of edge of actual electrode becomes less pronounced. We expect that further current rise will lead to further expansion of the cathode spot.

Fig.12 through Fig.14 demonstrates spatial distributions of main flow characteristics. Fig.15 through Fig.19 shows distributions of the flow variables along the discharge axis. Four new features of the flow should be noticed. First, the bow shock stand-off distance increases as total current increases. In addition, the serious modification of the front surface occurs. At high current the flow around a blunt cylinder looks like the flow around a cone. Second, the re-circulation zone always takes place in the shock layer. Third, the flow in the discharge channel (zone between anode and the bow shock) is characterized by diminished values of Mach number. This is due the temperature rise because of Joule heating. Forth, the level of static pressure at the cathode surface is much lower than those observed in discharge-off case (see Fig.16 and Fig.19). This should result in significant reduction of gasdynamic drag as will be shown later. These calculations show that effect of the discharge on the flow structure is due to heat release from the electronic current flowing in the main part of the discharge channel. Principal fact, according to, for example, [3] is that the power is inputted in front of the bow shock. This actually decreases Mach number of oncoming flow. Role of the heat release due to ionic current within the cathode layer will be discussed later.

Fig.20 represents several integral characteristics of the discharge: voltage-current characteristics (curve 1), net discharge power normalized by the reference value $Q_0 = 1/2\rho_0 U_0^3 S_m$ (curve 2), and the total drag normalized by the reference value $D_0 = 1/2\rho_0 U_0^2 S_m \cdot C_x$ (curve 3). Here ρ_0 is the density in free-stream flow, U_0 is the free-stream velocity, $S_m = \pi r^2$ is the cylinder cross-section, r is cylinder radius. Free-stream energy flux is $Q_0 = 134\text{W}$, the free-stream drag coefficient is $C_x = 1,014$. Note once again that in current calculations strong changes in flow structure are caused by the thermal effects only: role of the space charge and related force appeared to be small. It should also be noticed that heating from the flowing current is quite effective. For example, adding to the flow of 25% of the reference energy results to almost two-fold decrease in drag.

As has been shown the Joule heating is the primary effect which changes the flow around a cylindrical cathode. At the same time there are three parts of the discharge in which total heat rate differs significantly, see Fig.17: near-anode zone in which Joule heat rate values are high due to constriction of current at small electrode surface; main zone of the channel in which the lowest heat rates are observed; and shock layer together with cathode layer where the heat rates have maximum values. Which part of the discharge is most responsible for the flow modification? To answer this question two test problems have been solved. In the first problem the contribution of electronic current to heat release has been canceled. In the second one the ionic contribution has been canceled. Both cases start with flow and plasma fields obtained in regular case: $E = 2100\text{V}$, $U = 763\text{V}$, $I = 44.6\text{mA}$. Distributions of pressure and temperature along the discharge axis presented in Fig.21 (see also Figs.16 and 17) show that effect of plasma on the flow is due to heat release in supersonic part of the flow, which, in turn, is due to electronic current contribution. In opposite case the flow structure is almost undistinguishable from the original (no discharge) flow structure. In this case the total drag reduction is only 3% while total energy input is $Q_e/Q_0 = 0.26$. In the second case the flow within shock layer changes essentially. As well, the plasma variables distributions within shock layer differ from those obtained in the regular case,

see Fig.22. At the same time, surface distribution of pressure and total drag remain the same as in regular case.

Conclusions

Coupled flow-plasma model developed in paper¹ has been applied to numerically study longitudinal electric discharge in supersonic flow ($Ma = 3.2$) investigated experimentally in paper³. Attention has been paid to effect of plasma on the neutral gas flow and, specifically, to effect of distribution of heat release on plasma and flow characteristics.

In general, there is a qualitative agreement of the calculated discharge with the experimental one: shape of the discharge, its influence on the flow, level of currents and voltages are similar to those reported in paper³. Conditionally, four main parts of the discharge channel can be distinguished: near-anode part of almost quasi-neutral plasma; main part of the plasma column, which spreads up to the front of the bow shock; zone of plasma within a shock layer; and the cathode layer of size of 0.5 – 1 mm. Whereas concentration of charged particles grows with current in all discharge zones, concentrations, electric field strength and ionic current density at the cathode surface diminish as current increases. At the same time the size of cathode spot i.e. current-taking part of the cathode surface increases.

It has been found that discharge has a strong influence on the flow. This is expressed in significant increase of the bow shock stand-off distance, in strong modification of the front of bow shock, and in a strong reduction of pressure over a cathode surface. As consequence, significant reduction of gas dynamic drag was observed. The only mechanism of such a strong influence of the discharge was found to be a heat release in supersonic part of the discharge due to electronic current. Intensive heating in a cathode layer due to contribution of ionic current is of secondary importance. This modifies a flow and plasma field within the shock layer while the position of the shock, the level of pressure in the shock layer and at the surface and the drag are determined by the plasma upstream the bow shock. As in paper¹, effect of electric force in the near-cathode positively charged layer appeared to be negligible.

The same thermal mechanism was found to be responsible for the influence of the discharge on the flow in calculations carried out in paper¹. However, unlike experimental work² this influence turned out rather small. The reason of disagreement of computational and experimental observations seems to lie in original flow field. The flow coming on the model was reported (in paper²) to be supersonic while in computations¹]it was transonic with a large recirculation zone in front of the model. Inputting power to such flow was shown to be ineffective (see also paper⁴) Basing on the results of the current work one can assume that if the supersonic flow were considered in paper¹, similar to paper² significant drag reduction was obtained due to heat release in supersonic part of the discharge column.

References

1. Bityurin V.,Bocharov A., and Popov N. Numerical Simulation of the Discharge in Supersonic Flow Around a Sphere// Paper 2007-0223. Proc. 45th AIAA Aerospace Sciences Meeting & Exhibit, 5-8 January 2007, Reno, NV.

2. Klimov A., Bityurin V., Kuznetsov A., Vystavkin N., Vasiliev M. External and Combined Plasma Discharge in Supersonic Airflow // Paper 2004-0670. Proc. 42nd AIAA Aerospace Sciences Meeting & Exhibit, 4-8 January 2004, Reno, NV, p.5.
3. Fomin V.M., de Roquefort Th.A., Lebedev A.V., Ivanchenko A.I. Supersonic flows with longitudinal glow discharge // Proc. of III International Workshop on Magneto-Plasma Aerodynamics in Aerospace Applications. Ed. V.A. Bityurin. Moscow. IVTAN. 2001. P. 66-72.
4. Georgievsky P.Yu., Levin V.A., Supersonic Flow Control by Localized Energy Input, J. Mech. Fluid and Gas, No.5, pp.152 – 165, 2003 (in Russian).

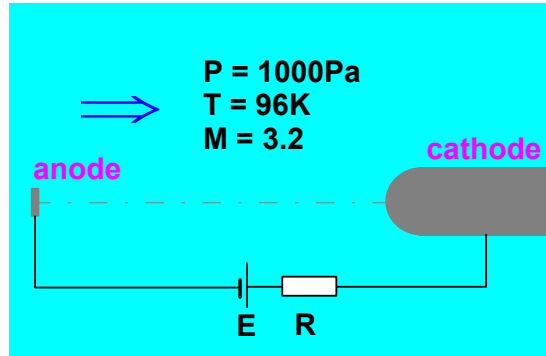
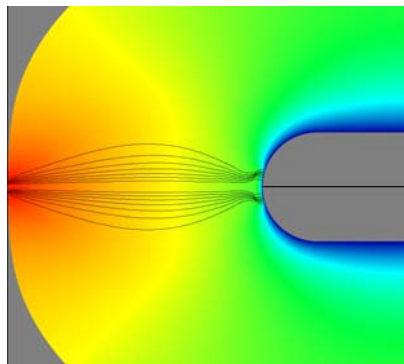
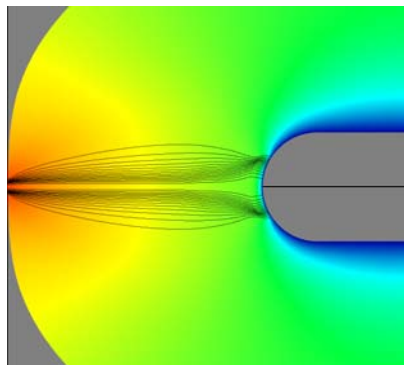


Fig.1. Layout of computational domain.

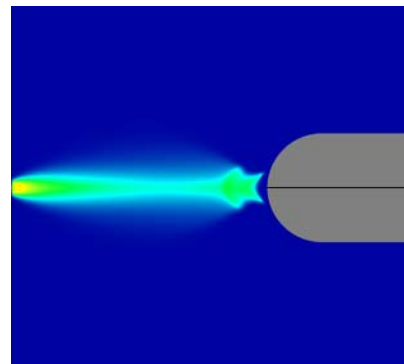


I = 21 mA

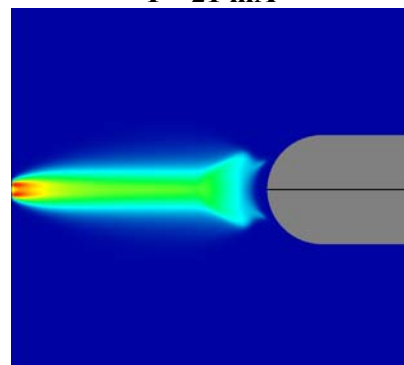


I = 44 mA

Fig.2. Electric potential distribution (filled) and total current stream lines.



I = 21 mA



I = 44 mA

Fig.3. Electron number density, $N_e^{max} = 2.85 \cdot 10^{12} \text{ cm}^{-3}$

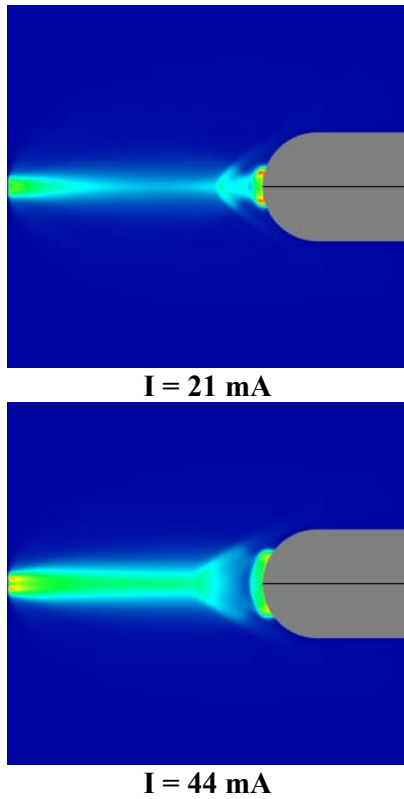


Fig.4. Ion number density, $N_i^{max} = 3.92 \cdot 10^{12} \text{ cm}^{-3}$.

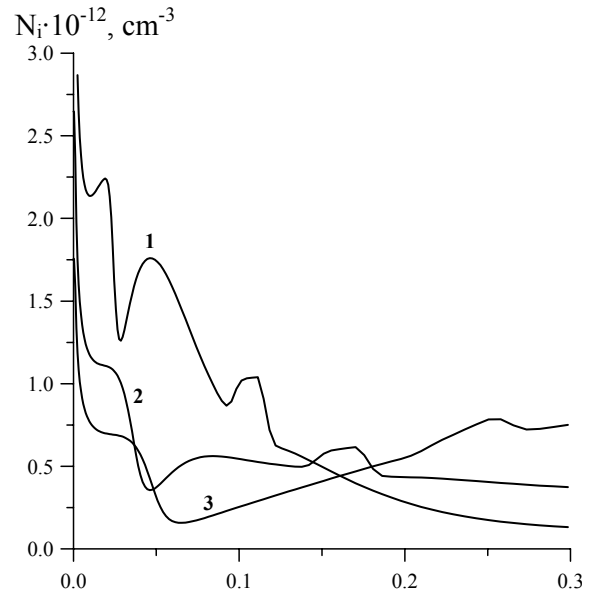


Fig.6. Distribution of ion number density along the symmetry line near the cathode. 1 - $I=7\text{mA}$, 2 - $I=21\text{mA}$, 3 - $I=44\text{mA}$. Cathode - left. Inter-electrode gap is 14 mm.

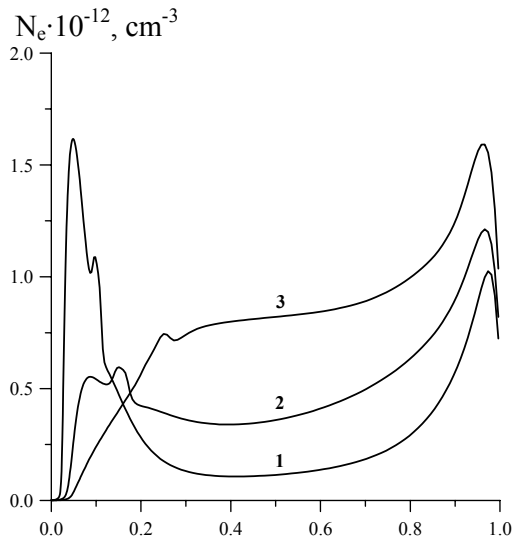


Fig.5. Distribution of electron number density along the symmetry line. 1 - $I=7\text{mA}$, 2 - $I=21\text{mA}$, 3 - $I=44\text{mA}$. Cathode - left. Inter-electrode gap is 14 mm.

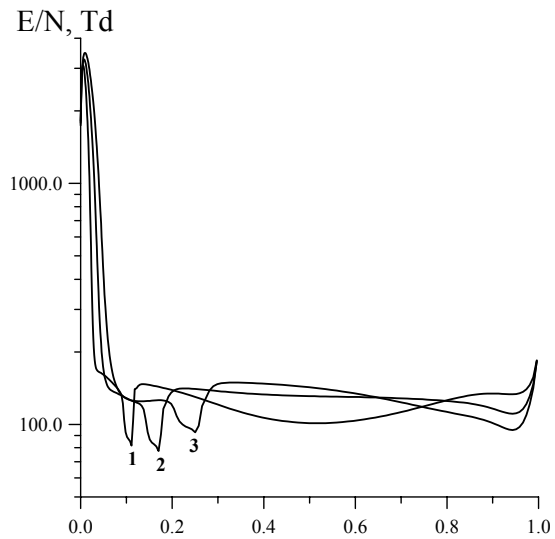


Fig.7. Distribution of reduced electric field E/N along the symmetry line. 1 - $I=7\text{mA}$, 2 - $I=21\text{mA}$, 3 - $I=44\text{mA}$. Cathode - left. Inter-electrode gap is 14 mm.

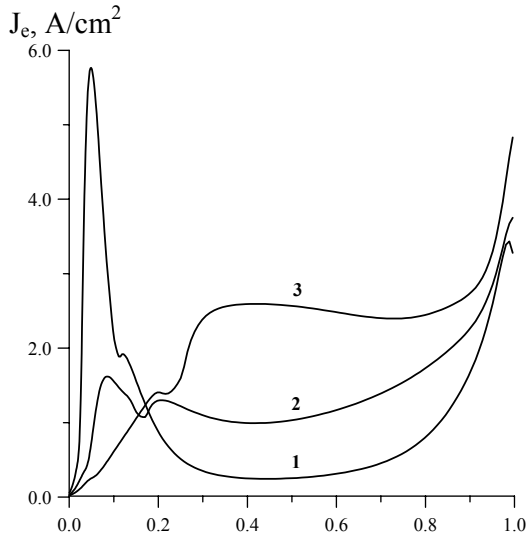


Fig.8. Distribution of electron current density along the symmetry line. 1 – $I=7\text{mA}$, 2 – $I=21\text{mA}$, 3 – $I=44\text{mA}$. Cathode - left. Inter-electrode gap is 14 mm.

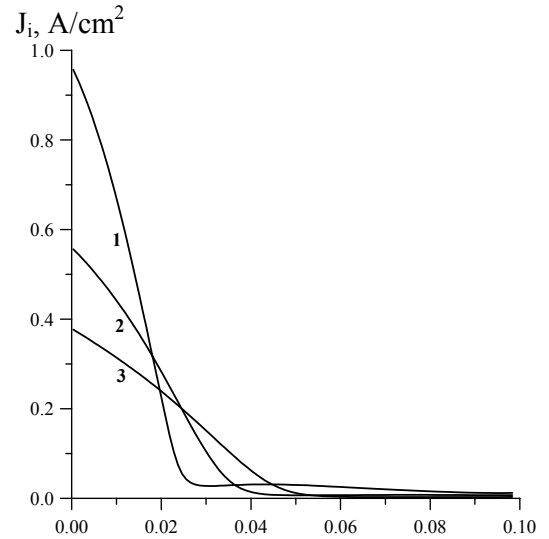


Fig.9. Distribution of ion current density along the symmetry line near the cathode. 1 – $I=7\text{mA}$, 2 – $I=21\text{mA}$, 3 – $I=44\text{mA}$. Cathode - left. Inter-electrode gap is 14 mm.

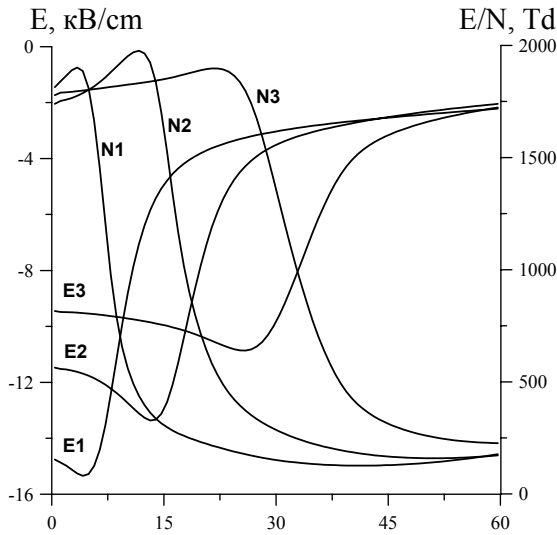


Fig.10. Distribution of electric field strength ($E1$, $E2$, $E3$) and reduced electric field ($N1$, $N2$, $N3$) over the cathode surface. 1 – $I=7\text{mA}$, 2 – $I=21\text{mA}$, 3 – $I=44\text{mA}$. Surface coordinate is given in degrees.

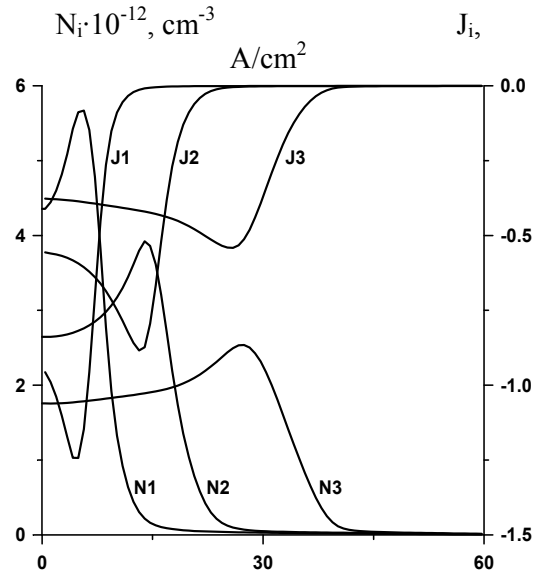


Fig.11. Distribution of ion number density ($N1$, $N2$, $N3$) and ion current density ($J1$, $J2$, $J3$) over the cathode surface. 1 – $I=7\text{mA}$, 2 – $I=21\text{mA}$, 3 – $I=44\text{mA}$. Surface coordinate is given in degrees.

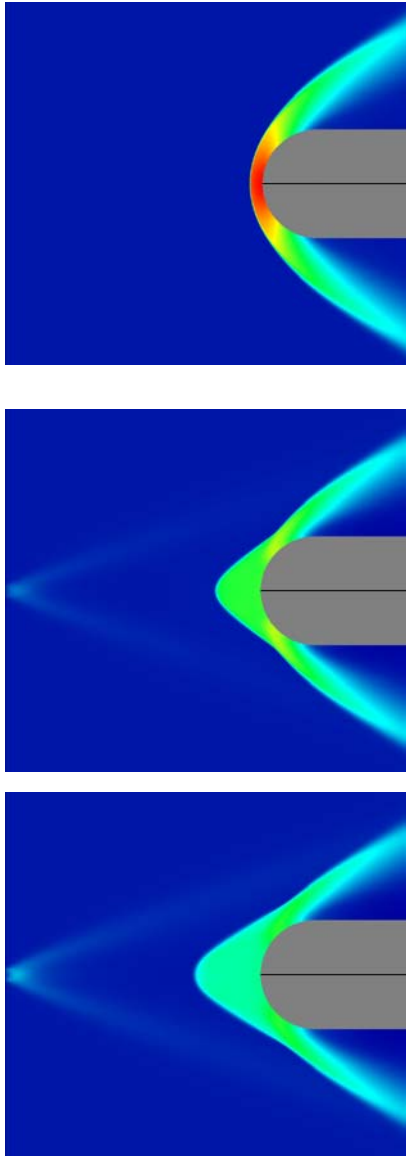


Fig.12. Pressure: $I=0$ (top), $I=21\text{mA}$ (mid), $I=44\text{mA}$ (bottom). $P_{min} = 855\text{Pa}$, $P_{max} = 13860\text{Pa}$.

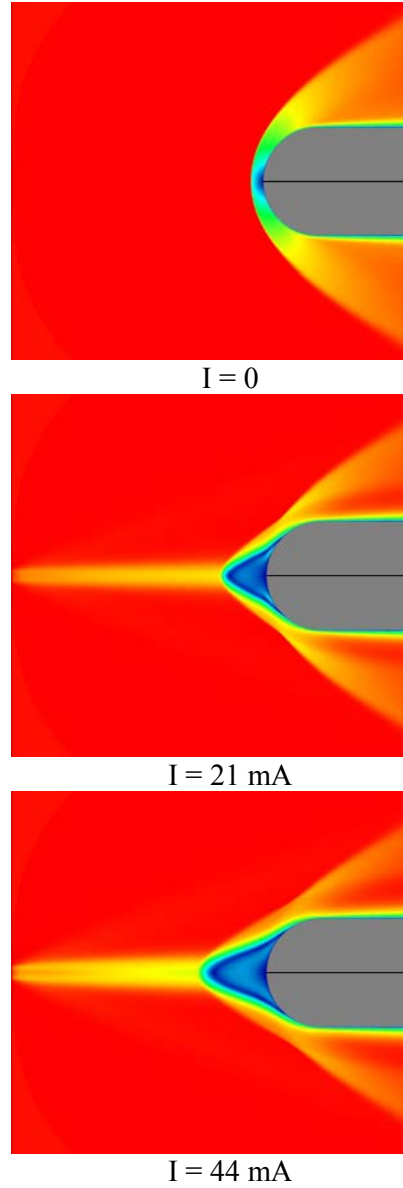


Fig.13. Mach number: $I=0$ (top), $I=21\text{mA}$ (mid), $I=44\text{mA}$ (bottom). $M_0 = 3.2$.

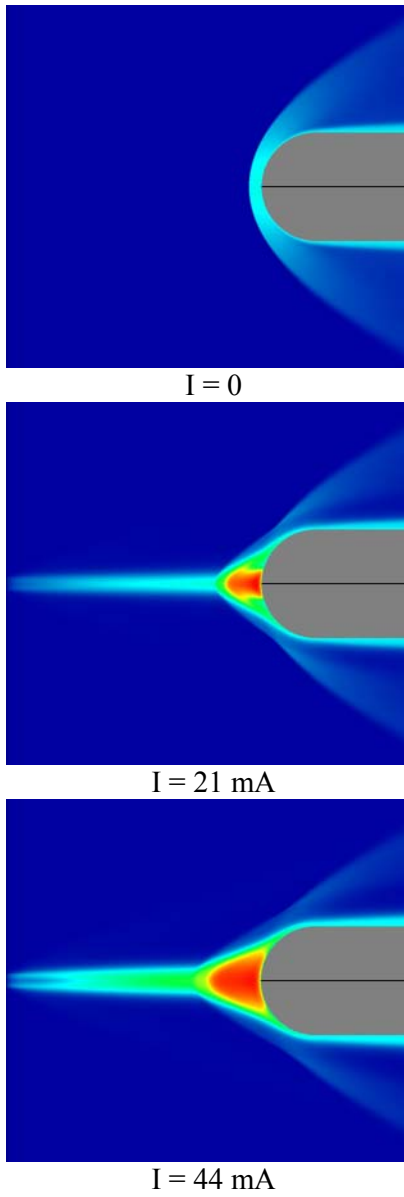


Fig.14. Temperature: $I=0$ (top), $I=21\text{mA}$ (mid), $I=44\text{mA}$ (bottom). $T_{min} = 96\text{K}$, $T_{max} = 1570\text{K}$.

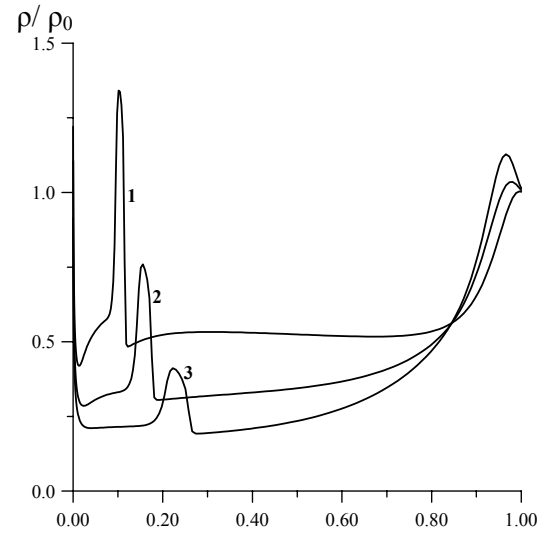


Fig.15. Distribution of density along the symmetry line. 1 – $I=7\text{mA}$, 2 – $I=21\text{mA}$, 3 – $I=44\text{mA}$. Cathode - left. Inter-electrode gap is 14 mm.

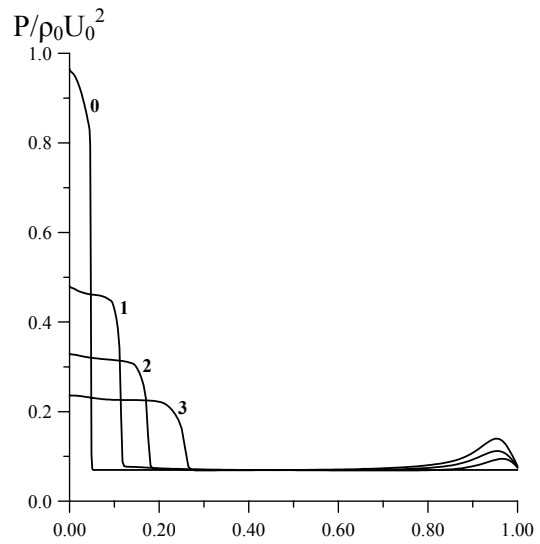


Fig.16. Distribution of pressure along the symmetry line. 1 – $I=7\text{mA}$, 2 – $I=21\text{mA}$, 3 – $I=44\text{mA}$. Cathode - left. Inter-electrode gap is 14 mm.

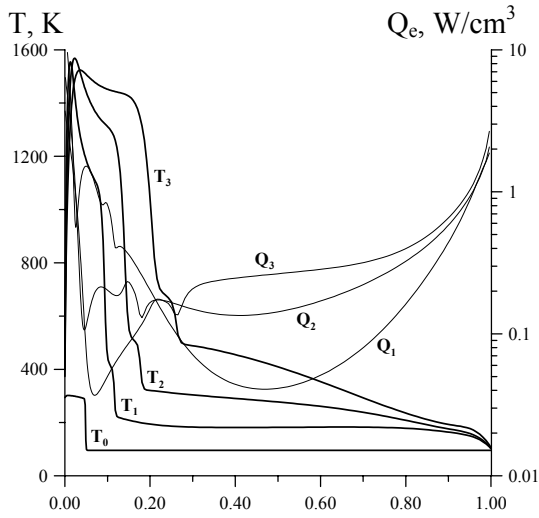


Fig.17. Distribution of temperature (T_0, T_1, T_2, T_3) and heat power density (Q_1, Q_2, Q_3) along the symmetry line. 1 – $I=7\text{mA}$, 2 – $I=21\text{mA}$, 3 – $I=44\text{mA}$. Cathode - left. Inter-electrode gap is 14 mm.

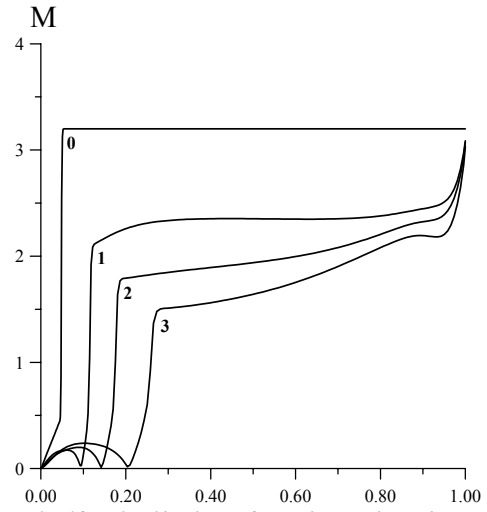


Fig.18. Distribution of Mach number along the symmetry line. 1 – $I=7\text{mA}$, 2 – $I=21\text{mA}$, 3 – $I=44\text{mA}$. Cathode - left. Inter-electrode gap is 14 mm.

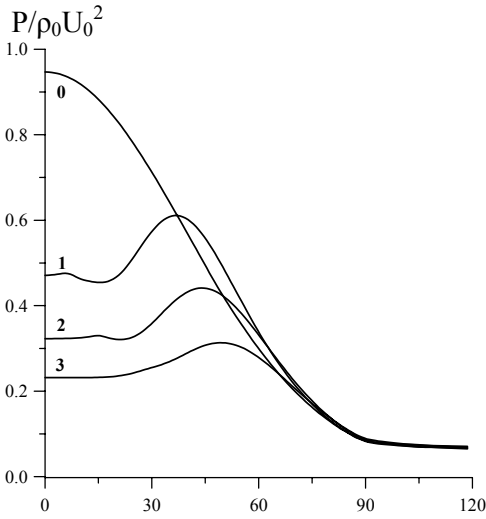


Fig.19. Distribution of pressure over the cathode surface. 0 – $I=0$, 1 – $I=7\text{mA}$, 2 – $I=21\text{mA}$, 3 – $I=44\text{mA}$. Surface coordinate is given in degrees.

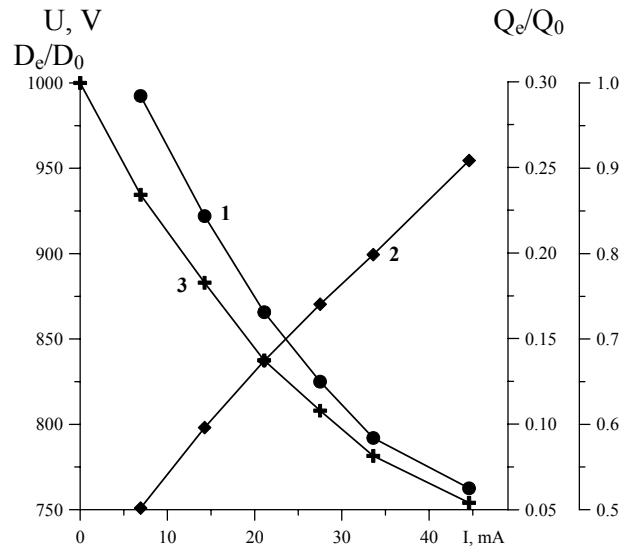


Fig.20. Voltage-Current characteristics (1), heat power input Q_e/Q_0 (2) and total drag D_c/D_0 (3). $Q_0 = 1/2\rho_0 U_0^3 S_m$, $D_0 = 1/2\rho_0 U_0^2 S_c$.

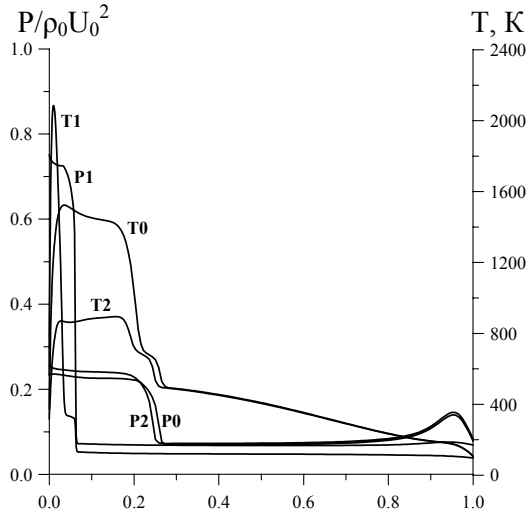


Fig.21. Distribution of pressure (P_0, P_1, P_2) and temperature (T_0, T_1, T_2) along the symmetry line for three cases of heat release: 0: $Q = (J_e + J_i)E$, 1: $Q = J_iE$, 2: $Q = J_eE$.

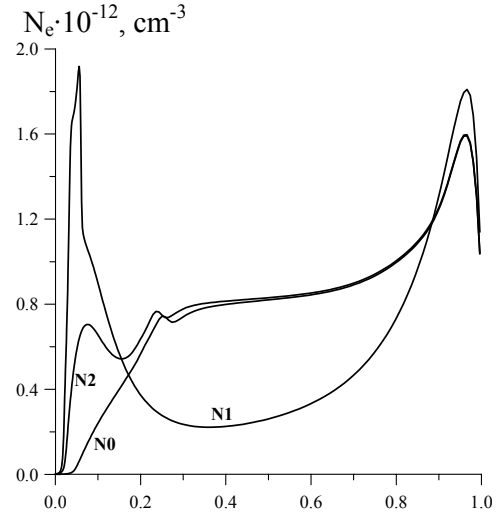


Fig.22. Distribution of electron number density (N_0, N_1, N_2) along the symmetry line for three cases of heat release: N_0 : $Q = (J_e + J_i)E$, N_1 : $Q = J_iE$, N_2 : $Q = J_eE$.